Research Article

Wang Yonggui, Wu Jiangjiang, and Zhang Juan*

Study on the mechanical properties and microstructure of recycled concrete reinforced with basalt fibers and nano-silica in early low-temperature environments

https://doi.org/10.1515/ntrev-2023-0185
received October 2, 2023; accepted December 20, 2023

Abstract: The effects of basalt fibers (BF) and nano-silica (NS) on the mechanical properties and microstructure of recycled concrete (RC) in early low-temperature environments were investigated by placing the BF and NS modified RC specimens in the environments of −20, −10, 0, and 25°C for curing for 6 h, followed by standardized maintenance. The damage morphology and mechanical properties of modified RC were analyzed in such environments. The formulae for the compressive strength of RC, which was affected by BF and NS, were fitted using statistical product and service solutions, and a micromorphological analysis of the modified RC was conducted using scanning electron microscope. The mechanical properties of RC decreased owing to the influence of early low temperatures, among which 0°C caused the largest damage crack and the most serious effects. In the early low-temperature environments, the physical properties of RC generally increased and then decreased with the increase in BF dosage; however, increasing NS dosages improved its mechanical properties. The composite doping of BF and NS was more obvious than the single doping of BF or NS to enhance the performance of RC, and the internal pore structure was considerably improved. The preferred doping amounts were 3 kg m^{-3} of BF and 2% NS.

Keywords: recycled concrete, nano-silica, mechanical properties

*** Corresponding author: Zhang Juan,** Energy Economic Research Center, Henan Polytechnic University, Jiaozuo, 454000, China, e-mail: zjuan0420@sina.com
Wang Yonggui, Wu Jiangjiang: School of Civil Engineering, Henan Polytechnic University, Jiaozuo, 454000, China

1 Introduction

In the twenty-first century, construction development moved to a new stage. Green sustainability has gained importance, and the disposal of waste concrete produced by the construction and demolition of buildings has become a major problem. One of the solutions is to utilize waste concrete as a recycled aggregate (RA) instead of natural aggregate (NA) in construction [1,2]. According to statistics, the annual building growth in China is approximately 3.182 billion square meters, and the output of structural waste is as high as 460 million tons [3]. Malaysia produces approximately 26,000 tons of construction waste per day with a recycling rate of only 15%, which is considerably lower than that in developed countries such as Singapore and Germany [4]. Studies have shown that the strength of recycled concrete (RC) is 88.4% that of ordinary concrete [5]. Consequently, the preparation of high-performance RC has become a realistic requirement, and admixtures have been added to prepare high-performance RC [6].

According to a previous study, fibers can significantly improve RC performance [7]. Basalt fibers (BF) are a new type of inorganic fiber produced by melting volcanic rocks and are superior to other fibers in terms of lower cost and material properties [8]. The correct amount of BF was evenly dispersed in the concrete without agglomeration [9]. Yuan *et al.* [10] tested the length and amount of BF, and the results indicated that the toughness of the matrix was significantly correlated with the BF length and dosage. Zheng *et al.* [11] analyzed the effect of nano-silica (NS) and BF on the mechanical properties of RC and found that BF significantly affected the connection between various matrices inside RC, whereas NS effectively increased its compactness with an optimal concentration of 2%. Fang *et al.* [12] analyzed the elastic modulus and physical properties of RC with different BF doping levels and found that BF increased the toughness of RC with optimal BF volume

fractions of 0.2 and 0.1%. The BF analysis of sea sand concrete conducted by Yang *et al.* [13] showed that it effectively enhanced its bending and compression properties. Zheng *et al.* [14] controlled the length and content of BF to analyze the influence of BF on the physical properties of RC and observed that the increase in compressive strength of RC with the BF length was slightly lower. However, a BF length of 12 mm was conducive to the cleavage tensile and bending properties. Chen *et al.* [15] analyzed the impact of BF on the durability of concrete in seawater and observed that BF effectively reduced the tensile strength of seawater by bridging the aggregates in concrete. Zhang *et al.* [16] used scanning electron microscopy (SEM) to analyze the interfacial microanalysis of RC with BF. They observed that BF significantly improved the interface of RC when RC was replaced at 50%, as it effectively prevented RC from cracking and slowed crack development. Wang *et al.* [17] demonstrated that modifying BF with NS improved its surface roughness, which is more conducive to the influence of BF on RC structures.

Modern technological innovations provide more possibilities for improving RC, in which nanomaterials, such as NS [18], nano-TiO_2 [19], nano-Ca_2CO_3 [20], and nano-Al_2O_3 [21], have various applications. Yan *et al.* [22] used NS to prepare high-performance nano-concrete and demonstrated that NS improved the toughness of concrete and reduced its initial stiffness. Mukharjee and Barai [23] analyzed an RC interface admixed with NS using the Vickers microscope hardness test and backscattered SEM, indicating that the microstructure of RC doped with NS was effectively reduced, and more hydration products filled the pores. Said *et al.* [24] analyzed the impact of various NS dosages on the overall performance and observed that the incorporation of NS significantly improved the compactness of concrete and reduced porosity. Further, a more refined pore architecture was obtained at 6% NS. Nazari and Riahi [25] analyzed the mechanism of NS in reforming the attributes of concrete. The results indicated that NS acts as an infilling agent to fill the voids, and NS as a nanomaterial has high activity and a volcanic ash effect that accelerates the hydration reaction, resulting in smaller $Ca(OH)_2$ crystals. Zhang and Zhu [26] demonstrated that the reaction between NS and $Ca(OH)_2$ in concrete promoted the generation of hydration products and enhanced mortar adhesion. Rezaei *et al.* [27] showed that 4.5% NS effectively reduced the proportion of large pores in concrete, which significantly affected the compressive properties. Xu *et al.* [28] showed that NS improved the interface transition zone (ITZ) and microstructure by reducing the internal defects in concrete through the filling effect and promoting the hydration reaction. Vijayan *et al.* [29] mixed NS with silica fume into concrete to assay the bond intensity, and compressive intensity, and analyzed it microscopically using SEM and X-ray (CT) diffraction. The results showed that the intensity mixed with NS with the ITZ interface exceeded that of the silica fume and the bond intensity of the ITZ improved more than the compressive intensity with NS content. Wang *et al.* [30] mixed BF and NS with RC and demonstrated that NS favored the bonding of BF with cement and increased the ITZ properties of RC.

Most of the test environment of concrete was approximately at 20°C, which differed from that in the north or inland areas with large climate change. Yi *et al.* [31] analyzed the reasons for the decline in compressive intensity at low temperatures in the early stages and showed that the water on the concrete surface penetrated the interior through pores between the aggregates to form ice lenses. Thus, the water in the pores transforms from liquid to solid, leading to a decrease in water content in the slurry and the formation of small pores, which affects the development of strength and is related to the stress generated by the volume expansion of ice crystals inside the concrete. Xia *et al.* [32] analyzed the effect of NS on the early mechanical properties of concrete during winter construction and showed that NS promoted the early hydration of cement and effectively improved the properties of cementitious materials. Zhang *et al.* [33] analyzed the deformation law at low temperatures and designed a non-contact deformation test device used at negative temperatures; the results indicated that the transformation law of concrete at low temperatures was divided into six stages. Dong *et al.* [34] analyzed the relationship between the microstructure and micromechanical function of concrete at different negative temperatures and showed that the temperature decreased for pre-curing, sparser construction of the cement paste leading to a reduction in pore sizes to less than 20 nm, as well as the compressive strength. Dai *et al.* [35] studied the concrete at low temperatures and measured its mass loss and peak stress-strain before and after it was subjected to low temperatures. The results showed that low-temperature curing hindered the hydration reaction, forming frost heave cracks between the mortar and aggregate. Thus, its physical properties declined, and a high water-cement ratio severely affected the concrete at low temperatures. To study the microscopic mechanism of concrete damage and reveal the causes of its cracking, the development of microscopic crack porosity within the concrete was analyzed by SEM [14], mercury intrusion porosimetry [36], and CT [37].

The aforementioned examples indicate that research on early low-temperature concrete has primarily focused on freeze–thaw cycles [38,39] and the freeze–thaw damage

caused by low-temperature curing after the final setting [40,41]. However, the current research on RC in low-temperature environments focuses on the frost resistance analysis of RC under the influence of low temperatures after the maintenance cycle and the effect of freeze–thaw cycles on its mechanical properties. The mechanical properties of RC in the early stage when it is cast and subjected to low temperatures have not been adequately researched. The application of RC has also expanded in recent years, and construction and demolition waste have been gradually recycled and reused. However, during the alternation of seasons, such as from fall to winter or early spring, the sudden temperature drops and frost phenomena affect the physical properties of RC to varying degrees. Meanwhile, considering the excellent performance of BF and NS based on previous studies, this study improves RC with BF and NS and examines its physical properties at four temperatures, namely, 25, 0, −10, and −20°C in the early stage, and analyzes its micro-morphology using SEM.

2 Test survey

2.1 Materials

P.O. 42.5 silicate cement manufactured by Jiaozuo Qianye Cement Co. Ltd was used in the experiment. The initial and final setting times were 2.5 and 4 h, respectively. The specific chemical composition is shown in Table 1. The performance indexes of the cement were determined using Ordinary Silicate Cement (GB 178-2007). The aggregates comprised NAs and RAs, which were crushed and sieved using a jaw crusher after pouring the C40 concrete and maintaining for 28 days. Its physical properties are listed in Table 2, while the appearance of RA is shown in Figure 1. The fine aggregate used in the experiment was natural river sand with a fineness modulus of 2.86; its physical properties are shown in Table 3, and the particle size distribution curve is shown in Figure 1.

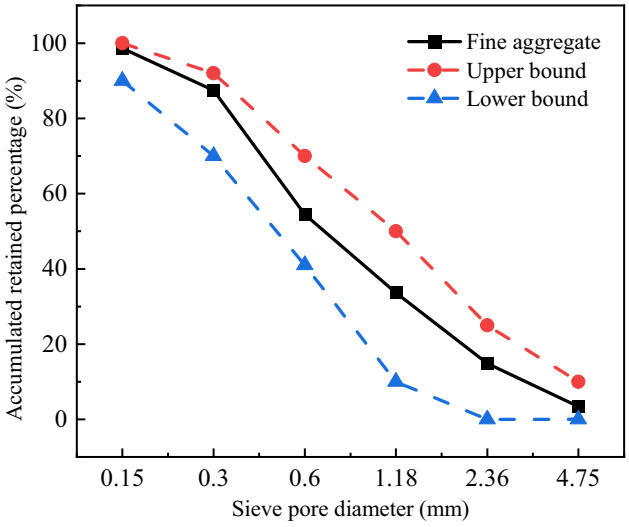

Figure 1: Particle size distribution.

The dopants used in these tests were BF and NS. The BF was provided by Jiangsu Nong Chaoer Composite Materials Co., Ltd. Its physical properties are listed in Table 4, while its appearance and morphology are shown in Figure 2. NS was selected from the NS dispersion of YC-SI01J produced by Xinan Chemical New Materials Co. Ltd. It had a PH of 9, solid content of 30%, and particle size of 10 nm. Tap water from Jiaozuo city was used.

2.2 Mixing design

For the experimental concrete ratios, the RA substitution rate and BF and NS admixtures were selected as the project alternating quantities. The RA substitution rates were 0 and 100%, while the BF admixtures were 0, 3, and 6 kg m^{-3}. The NS solid design was used in 0, 1, and 2% of the cases. Ten sets of working condition ratios were designed based on the above variables and the specific ratios are presented in Table 5.

To ensure a uniform distribution of BF and NS within the RC, the concrete was mixed using the segmental release method shown in Figure 3, as proposed by Ji [42]. The

Table 1: Chemical composition of the cement

Oxide	CaO	SiO_2	Al_2O_3	MgO	Fe_2O_3	SO_3
Mass (%)	65.40	21.00	21.00	3.40	2.80	2.00

Table 2: Physical properties of the coarse aggregate

Aggregate type	Particle size (mm)	Apparent density (kg m^{-3})	Bulk density (kg m^{-3})	Water absorption (%)	Crushing value (%)
NA	5–20	2,743	1,486	1.52	9.4
RA	5–20	2,537	1,325	5.85	16.4

Table 3: Physical performances of the fine aggregate

Performance index	Particle size (mm)	Apparent density (kg m^{-3})	Water absorption (%)
Specification requirements	<4.75	≥2,500	≤2.0
Fine aggregate	<4.75	2,768	1.3

Table 4: Physical properties of BF

Length (mm)	Diameter (μm)	Density (g cm^{-3})	Modulus of elasticity (GPa)	Tensile strength (MPa)	Fracture elongation (%)
12	13	2.64	91–110	3,000–4,800	2.6–3.3

coarse aggregate was soaked in water for 24 h before mixing, and then removed and dried to surface dryness before mixing with the RC.

2.3 Sample preparation

The poured RC was placed into a 100 mm × 100 mm × 100 mm plastic test piece on a vibrating table for 2 min. The specimen was then smoothed and placed in constant-temperature box for curing. To study the performance of concrete at low temperatures in the early stage, four temperatures (25, 0, −10, and −20°C) were selected as the early curing temperatures. The freshly poured test block was cured at the above temperature for 6 h, and then removed and cured in a standard room (20 ± 2°C, 95% relative humidity) for 7, 14, and 28 days. The cubic compression and splitting tensile tests were conducted according to GB/T 50081-2019 [43].

2.4 Test scheme

This study primarily involved testing the physical properties and studying the SEM microstructure of RC.

2.4.1 Mechanical performance test

A 600 kN electro-hydraulic servo press was used for testing. The trial procedure and data processing were performed according to GB/T 50081-2019 [43]. The mean value of three test blocks from each group was used for the analysis. A microcomputer was used to command the load-on rates of 0.5 and 0.05 MPa s^{-1} during the cubic compressive and splitting tensile tests, respectively.

Table 5: Mix ratio (kg m^{-3})

Specimen	Water	Cement	NA	RA	Sand	MBF	NS
NC	185	462.5	1255.7	0	576.8	0	0
RC	185	462.5	0	1139.6	536.3	0	0
B0N1	174.21	457.87	0	1139.6	536.3	0	15.42
B0N2	163.41	453.25	0	1139.6	536.3	0	30.83
B3N0	185	462.5	0	1139.6	536.3	3	0
B3N1	174.21	457.87	0	1139.6	536.3	3	15.42
B3N2	163.41	453.25	0	1139.6	536.3	3	30.83
B6N0	185	462.5	0	1139.6	536.3	6	0
B6N1	174.21	457.87	0	1139.6	536.3	6	15.42
B6N2	163.41	453.25	0	1139.6	536.3	6	30.83

Note: NS content is the nano-silica dispersion mass.

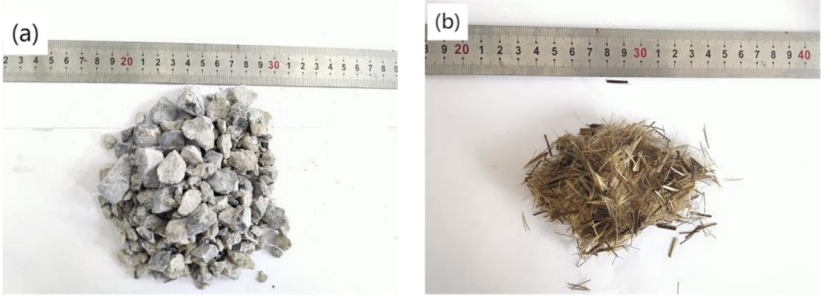

Figure 2: Images of (a) RA and (b) BF.

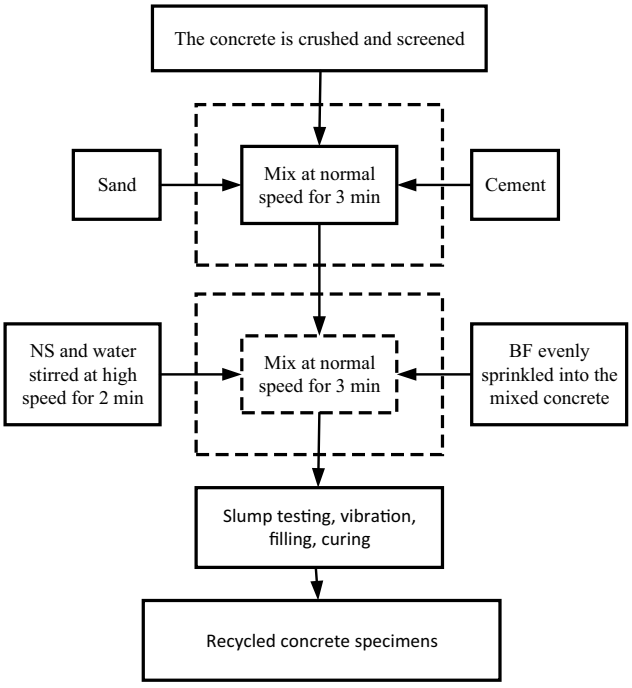

Figure 3: RC mixing process.

2.4.2 SEM microscopic test

The samples used in the test in this study were concrete, which underwent six steps before SEM studies, namely, sampling, cleaning, dehydration, drying, sticking samples, and spraying gold. Samples containing BF and possessing obvious interfaces were selected, and converted into 1 cm^3 specimens to ensure that the bottom was flat. The surface of the specimen was cleaned with distilled water, dehydrated with ethanol, and placed in a natural environment to allow the ethanol to evaporate completely and dry the specimen. After drying, the specimens were glued to the sample stage and coated with metal. The surface morphology of the sample was studied using field-emission electron microscope (Hitachi SU8220) to observe the microstructure of the bonding surface between the mortar and BF under various magnifications.

3 Test results and analysis

3.1 Experimental phenomena

3.1.1 Cubic compression test

The compressive damage corresponding to different BF dosages for 28 days in the early 0°C environment is shown in Figure 4. At 0 kg m^{-3} BF, cracks gradually appear on the surface of the RC test block with continued loading, finally leading to damage owing to penetrating cracks. The overall damage is severe, with the surface collapsing from the interior, and the aggregate and mortar separating. At 3 kg m^{-3} BF, the failure mode of B3N0 improved, and the surface layer of the test block detached; however, no aggregate separation and fragmentation occurred inside. The BF connected the aggregate and mortar, which weakened the influence of external forces on the test block. This is consistent with the results reported by Shatarat *et al.* [44]. At 6 kg m^{-3} BF, the improvement in the failure mode of B6N0 is the most significant, and no overall collapse is observed. The connection between the aggregates is good, and the widths and number of cracks are effectively reduced. Furthermore, the overall shape of the test block is maintained in good condition.

The compressive damages for different NS dosages at early −20°C for 28 days are shown in Figure 5. In the case of

Figure 4: Compressive failure mode for different BF contents: (a) RC, (b) B3N0, and (c) B6N0.

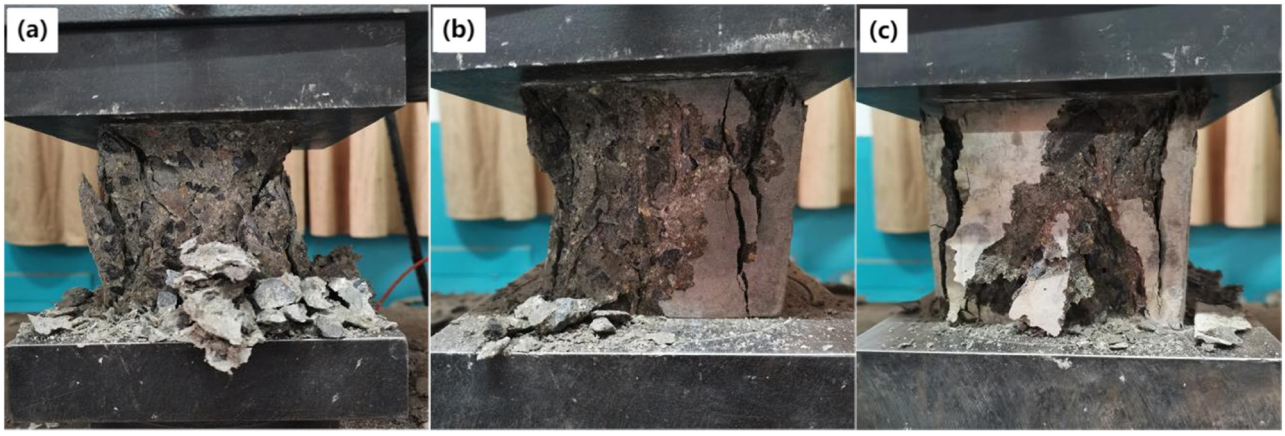

Figure 5: Compressive failure mode for various NS contents: (a) RC, (b) B0N1, and (c) B0N2.

0% NS, large diagonal penetration cracks appear inside the RC, accompanied by severe overall damage and a large amount of aggregate shedding. At 1% NS, the damage morphology of B0N1 improves; however, owing to the severe damage to the edges of the test block, collapse and vertical cracks occur. However, the overall internal morphology was relatively good, and there was no separation of the aggregate and mortar. At 2% NS, the overall shape of B0N2 is the best when damaged, with some surface parts damaged and cracks appearing. However, the number and width of cracks are effectively reduced. During compression failure, no large amount of aggregate shedding or holes was observed, which significantly improved the failure morphology compared with that corresponding to 0% NS. This was more consistent with the results reported by Nigam and Verma [45].

3.1.2 Splitting tensile test

A comparison of the splitting and tensile damage patterns of the specimens revealed the obvious effect of BF. The damage to RC with different BF dosages at an early temperature of −10°C for 28 days is shown in Figure 6. At 0 kg m^{-3} BF, the RC exhibits brittle damage with wide cracks. At 3 kg m^{-3} BF, B3N0 exhibits splitting tensile damage, the fibers on the intermediate fracture surface are pulled out by the external force, and the fracture surface is relatively intact without much damage. At 6 kg m^{-3} BF, the crack width on the rupture face of B6N0 decreases and the fiber-connected aggregate improves the overall damage pattern. As the BF doping increased, the integrity of the RC improved and the crack width reduced, improving the toughening performance of the RC. In the splitting tensile test, the

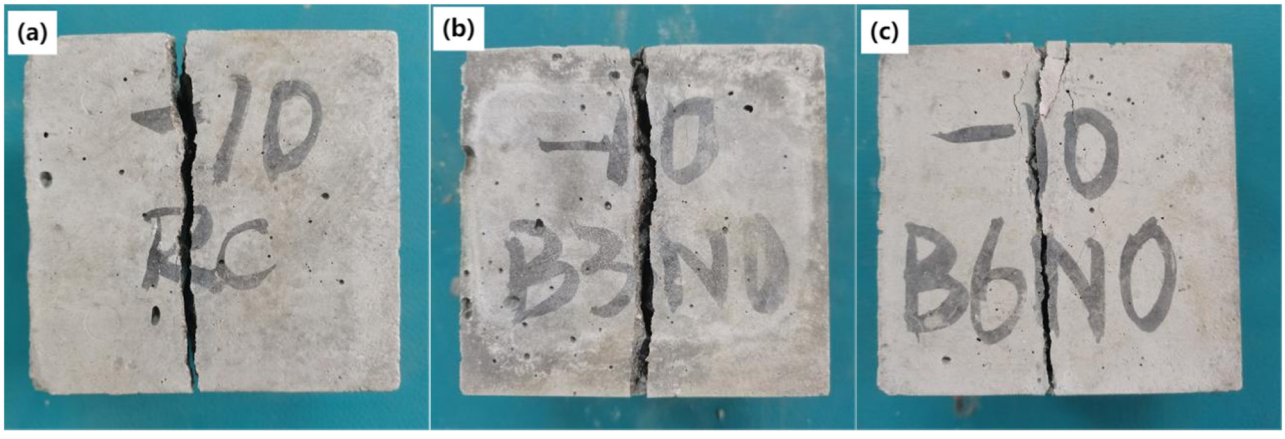

Figure 6: Splitting tensile failure mode: (a) RC, (b) B3N0, and (c) B6N0.

specimen was subjected to tensile stress concentrated on the middle-damaged surface. The fibers in the middle region acted as crack-blocking agents, which reduced the tensile stress inside the RC and improved its splitting tensile properties.

3.2 Analysis of mechanical properties

3.2.1 Cubic compressive strength

The mechanical performances of the test blocks in early low-temperature environments and the cubic compressive strength are listed in Table 6. NC was used as the test control group and its strength reached 39.48 MPa after 28 days of room temperature curing. The strength of the RC with a substitution rate of 100% was only 36.9 MPa after 28 days at 25°C, and its overall strength was lower than that of NC. This was consistent with the findings of Adessina *et al.* [46]. After crushing and screening, the aggregate was damaged; additionally, the old mortar on the appearance of the RA affected the physical properties of RC.

According to Table 6, which presents the changes in the cubic compressive strength in the early low-temperature environment, an early temperature of 0°C has the greatest impact on the compressive strength. The compressive strength affected the degree of cement hydration, at 0°C, when the water inside the concrete was not completely frozen in the state of ice-water mixture, can still be hydrated with the cement, but the hydration reaction inhibited by the inhibition of the initial setting time is delayed, after the initial setting of the low-temperature environment caused by the damage to the concrete internal part cannot be repaired, which led to the internal damage of the concrete in varying degrees, leading to the reverse of the cubic compressive strength. After curing at 0°C for 6 h and removing the specimens for standard curing, the unhydrated cement particles inside the concrete maintained the hydration reaction, and the strength of the concrete improved. Subsequently, the compressive strength increased with a decrease in the early ambient temperature. For example, in the early −10°C low-temperature environment, the compressive strength of the cube surpassed that of the early low-temperature environment at 0°C. This is because the negative temperature resulted in the conversion of water into ice inside the concrete, thereby preventing the occurrence of excessive hydration reaction at low temperatures standard maintenance, RC internal ice melting step-by-step, and the conversion of free water inside the concrete into ice caused by the damage to a certain extent of the repair. A lower curing temperature before the initial setting of concrete reduced the hydration reaction and delayed the initial setting time. As the temperature decreased to −20°C, the compressive strength of the concrete decreased compared to that at −10°C. The reason was analyzed primarily to be because of the existence of a large amount of water inside the freshly poured concrete. The water inside the concrete rapidly transformed into ice at low temperatures, which stopped the hydration reaction. Ice crystals appeared inside the concrete, and ice crystals from the adjacent pore space absorbed water to expand constantly. This increased the pore pressure inside the concrete, which coupled with the effect of the mortar and other fine aggregate led to the emergence and development of micro-cracks after the initial setting, and finally, reduced the cubic compressive strength of the concrete. In an early low-temperature environment of −20°C, the conversion of water into ice was accelerated, and the formation of ice crystals increased the expansion pressure over the early tensile strength of concrete. However,

Table 6: Compressive strength (MPa)

Specimens	7 days				14 days				28 days			
	25°C	0°C	−10°C	−20°C	25°C	0°C	−10°C	−20°C	25°C	0°C	−10°C	−20°C
NC	27.36	25.43	26.69	25.89	31.52	29.64	30.22	29.86	39.48	33.22	37.18	34.68
RC	27.34	24.02	26.42	25.29	30.23	26.96	28.99	28.39	36.69	32.29	35.84	34.49
B0N1	28.53	25.08	27.86	26.3	31.13	28.19	30.86	29.32	37.52	34.41	37.03	36.32
B0N2	29.34	26.51	28.79	27.38	31.76	29.35	31.43	30.35	37.64	35.04	37.52	37.04
B3N0	28.89	25.27	27.26	26.25	32.23	28.18	31.45	29.2	38.53	33.87	36.72	35.22
B3N1	30.51	27.53	29.56	29.09	32.53	29.94	31.25	30.35	39.08	35.65	38.03	37.56
B3N2	31.34	27.89	30.05	29.86	33.68	30.88	32.37	31.91	39.74	36.75	38.08	37.66
B6N0	27.66	25.74	26.86	25.76	31.05	27.93	29.48	29.19	37.01	34.55	36.25	34.86
B6N1	28.94	26.17	27.69	26.75	31.89	28.96	30.45	29.53	37.95	35.32	37.44	36.83
B6N2	29.95	26.47	28.86	28.05	32.07	29.95	30.87	30.02	38.34	36.36	37.86	37.22

the damage caused by frost was more serious. The concrete was then transferred for standard curing, before the initial set of damage repairs, but most of the damage cannot be repaired to form permanent damage, resulting in the internal structure of the loosening. With the increase in pressure during the cubic compression test, the presence of small internal cracks exacerbated the crack development at the aggregate interface.

Table 6 further shows that a BF of 3 kg m^{-3} enhances the compressive strength of RC most significantly. At early ambient temperatures of 25, 0, −10, and −20°C, the 28 days compressive strength of B3N0 was enhanced by 5.0, 4.9, 2.5, and 2.1%, respectively, compared with those of RC. BF forms a spatial lattice structure, which helps improve RC. An appropriate amount of BF can enhance the densification of RC, which further improves the overall performance of RC. The compressive strength of RC decreases owing to overdoping of BF. At the early ambient temperatures of 25, 0, −10, and −20°C, the 28 days compressive strength of B6N0 increased by 0.9, 7, 1.1, and 1, respectively, compared to those of RC, which is consistent with the analysis of Dilbas and Çakır [47]. This indicates that enhancing the compressive performance of RC by mixing large amounts of BF is undesirable. Under excessive BF doping, agglomeration occurs easily inside the RC, which is not conducive to the bonding between the aggregate and mortar because the coarse aggregate is unable to bear the pressure during the compression of cubic, and more defects appear locally.

Figure 7 shows the comparison of early strength development, and the compressive strength ratios of 7/28 days and 14/28 days with different BF dosages. The compressive strengths of the RC at 7 and 14 days reached approximately 70 and 80%, respectively, of the strengths at 28 days. The compressive strength was generally more rapidly developed at 7 days at 3 kg m^{-3} BF than at 0 and 6 kg m^{-3}. The early strength development of RC is influenced by temperature, and the optimum development of the physical properties of RC occurs at 25°C, which attains a maximum strength of 78.9% at 28 days. An early ambient temperature of −20°C has the greatest effect on the 7 days compressive strength of RC as the free water inside the RC transforms from liquid to solid and back again. The early hydration of RC is delayed, which hinders strength enhancement. With increased BF doping, the increase in the compressive strength at 7 days for early −20°C was insignificant, and the BF doping of 3 kg m^{-3} *vs* 6 kg m^{-3} increased by only 3.8 and 1.9% for B3N0 and B6N0 over RC.

As shown in Table 6, the compressive strength of the RC increases with the NS content, which agrees with the findings of Mukharjee and Barai [23]. As the NS nanoparticles were dispersed between the pores within the concrete as a filler to fill the pores, the RC specimens became denser. The $Ca(OH)_2$ crystals in the RC caused adverse effects during compression damage, and the volcanic ash effect of NS accelerated the hydration reaction to generate hydrated calcium silicate, which reduced the presence of Ca $(OH)_2$ crystals, as shown in equation (1). This phenomenon was confirmed by Roy *et al.* [48]. Therefore, the compressive strength of NS-doped RC was significantly improved.

$$SiO_2 + mH_2O + nCa(OH)_2 \rightarrow nCaO \cdot SiO_2 \cdot (m + n)H_2O. \quad (1)$$

As the temperature decreased to a negative value, the NS-doped RC exhibited improved compressive strength. At negative temperatures, the water freezes, and NS cannot exert its effect when transferred to the standard curing room. The ice gradually melted, and the temperature effect of NS became evident, which promoted the hydration of the cement. The concrete developed from the initial to the final set repaired the damage of the concrete caused by the negative temperature before the initial set and avoided

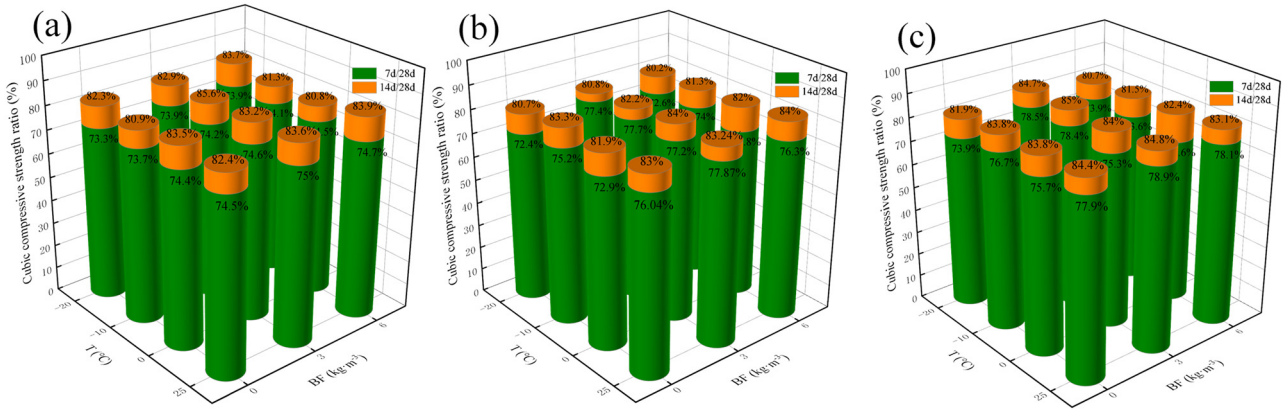

Figure 7: Relative compressive strength ratios for various BF contents: (a) 0% NS, (b) 1% NS, and (c) 2% NS.

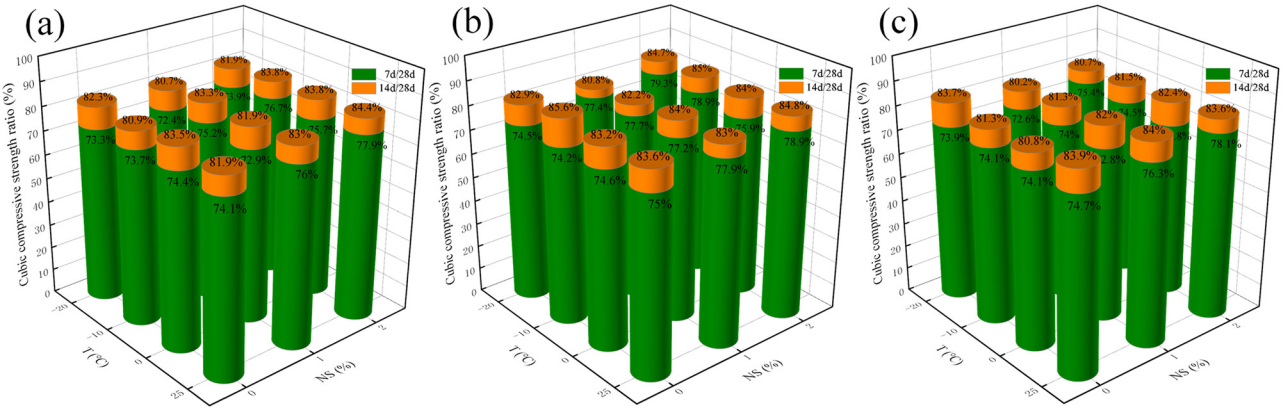

Figure 8: Relative compressive strength ratios for different NS contents: (a) 0 kg m^{-3} BF, (b) 3 kg m^{-3} BF, and (c) 6 kg m^{-3} BF.

the large number of micro cracks within the RC that degraded the compressive properties. Figure 8 shows the ratio of compressive strength at 7/28 days *vs* 14/28 days when NS doping is present. With the increase in NS doping, the early strength of the RC improved significantly and showed a general increasing trend. In the early environment of 25°C, the 7 days compressive strengths of B0N1 and B0N2 grew by 4.4 and 7.3%, respectively. The 7 days compressive strengths of B0N2 at 0, −10, and −20°C decreased by 9.6%, respectively, compared with that obtained at 25°C for BF doping of 0 kg m^{-3}, 1.9, and 6.7%. The volcanic ash effect of NS was mainly affected by the low temperature in the early stage, and it was gradually exerted when the RC was transferred for standard maintenance. However, the effect was not obvious. The hydration reaction of NS continued, RC densification increased, and physical properties improved.

Table 6 shows that the combined doping using BF with NS is more favorable for improving the RC compressive strength than single doping. This was consistent with the findings of Harish *et al.* [49]. The highest cubic compressive strength of RC was obtained when 3 kg m^{-3} BF and 2% NS were compounded. For 0°C, the compressive strengths of B3N0 and B0N2 were enhanced by 4.7 and 8.5%, respectively, over that of RC for single doping of 3 kg m^{-3} BF with 2% NS, and the compressive strengths of B3N2 were enhanced by 13.8% over that of RC for double doping of 3 kg m^{-3} BF with 2% NS. This is because the filling and volcanic ash effects of NS increased the internal compactness of RC and reduced the number of internal defects, which supported the realization of the bridge effect of BF and stronger ITZ performance. Excessive BF increased the internal defect content of the RC and lowered the final compressive strength.

3.2.2 Splitting tensile strength

The splitting tensile strength at different temperatures is shown in Table 7.

According to Table 7, the early 0°C environment has the most influence on the splitting strength. The 28 days splitting strength of RC decreases by 5.1% in the 0°C early low-temperature environment compared with that observed

Table 7: Splitting tensile strength (MPa)

Specimens	7 days				14 days				28 days			
	25°C	0°C	−10°C	−20°C	25°C	0°C	−10°C	−20°C	25°C	0°C	−10°C	−20°C
NC	3.02	2.24	3.01	2.76	3.21	2.94	3.16	3.01	3.52	3.28	3.48	3.45
RC	2.83	2.16	2.8	2.7	2.96	2.47	2.88	2.81	3.12	2.97	3.07	2.99
B0N1	2.75	2.41	2.67	2.63	3.19	2.99	3.15	3.08	3.38	3.06	3.28	3.15
B0N2	3.02	2.38	2.93	2.81	3.10	2.94	3.01	3.13	3.37	3.07	3.29	3.35
B3N0	3.01	2.44	2.96	2.77	3.25	2.99	3.04	3.2	3.42	3.24	3.48	3.27
B3N1	2.99	2.55	2.95	3.2	3.29	3.03	3.12	3.02	3.55	3.49	3.52	3.67
B3N2	2.97	2.58	2.87	2.98	3.36	3.02	3.14	3.09	3.62	3.35	3.57	3.43
B6N0	2.96	2.36	2.67	2.45	3.02	2.66	2.98	2.86	3.25	3.05	3.15	3.09
B6N1	2.82	2.39	2.63	2.56	3.12	2.68	3.03	2.96	3.48	3.19	3.47	3.25
B6N2	2.93	2.46	2.85	2.63	3.11	2.76	3.02	2.84	3.56	2.98	3.41	3.02

for 25°C. However, at −10 and −20°C, the splitting strength improves by 3.4 and 0.7%, respectively, compared with the value at 0°C. The low-temperature environment deeply affected the hydration reaction of cement, which internally damaged the concrete. This agrees with the phenomenon reported by Zhang *et al.* [50]. In the early environment of 0°C, the 7, 14, and 28 days splitting tensile strengths of B3N0 increased by 13, 21, and 9.1%, respectively, compared with those of RC when 3 kg m^{-3} BF was doped alone. The 7, 14, and 28 days splitting tensile strengths of B6N0 increased by 4.6, 7.7, and 2.7%, respectively, compared with those of RC when 6 kg m^{-3} BF was doped alone. These results show that a moderate amount of BF favors RC reform. During the early stage of loading, most of the load was borne by the aggregate mortar, and as the loading progressed, the microcracks gradually expanded the tensile stress to be transferred to the BF. Thus, the splitting tensile strength improved; however, excessive BF reduced the RC splitting tensile strength because it increased the amount of defects in the RC. This agrees with the results of Zhu *et al.* [51], who studied the effect of fibers on the RC splitting tensile strength.

Table 7 shows that although NS improves the splitting tensile strength of RC, the increase is smaller than that obtained using BF. In the early environments of 0 and −10°C, the 28 days splitting tensile strengths of B0N1 increase only by 3 and 6.8%, respectively, which is much smaller than that of BF on the cubic compressive strength. The influence of splitting tensile properties was more significant when BF and NS were doped together in RC. For example, in the early −10°C environment, the splitting tensile strength of B3N2 with 3 kg m^{-3} BF and 2% NS increased by 16.3% compared with that of normal RC, indicating that BF and NS have a better synergistic influence on the mechanical properties of RC.

4 Statistical product and service solutions (SPSS) analysis

Khodair *et al.* [52] developed a linear regression model using a statistical analysis software (SPSS) to derive an equation for the compressive strength of the RA replacement ratio, silica fume, mineral powder, and fly ash, as shown in equation (2).

$$f_{cu} = A_0 + A_1X_{RAC} + A_2X_{FA} + A_3X_{SL} + A_4X_{SF}. \quad (2)$$

where f_{cu} is the compressive strength; A_0, A_1, A_2, A_3, and A_4 are the parameters; X_{RCA} is the RA substitution rate; and X_{FA}, X_{SL}, and X_{SF} are the dosages of fly ash, mineral powder, and silica fume, respectively. Based on the above theoretical formula for the compressive strength, combined with the test data, the formula for the compressive strength of RC incorporating BF and NS doping in an early low-temperature environment was derived using SPSS, as shown in equation (3).

$$f_{cu,28} = A_0 + A_1X_{BF} + A_2X_{NS} + A_3X_{BF}^2 + A_4X_{NS}^2. \quad (3)$$

where $f_{cu,28}$ is the 28 days cubic compressive strength, while X_{BF} and X_{NS} are the dosages of BF and NS, respectively. The nonlinear regression model of SPSS was used to obtain the formula for the RC compressive strength under different early temperature environments along with the analysis of variance, as shown in Table 8. The corresponding results are shown in Figure 9.

Table 8 shows that the test data are in better agreement with the regression analysis data, and the correlation coefficient is large. Therefore, Table 8 can be used to predict the compressive strengths of the BF and NS composite-modified RC at different ambient temperatures.

The relationship between the splitting tensile strength and compressive strength of concrete [12] indicates that the splitting tensile strength can be converted from the compressive strength. The conversion equation between the concrete splitting tensile strength and cubic compressive strength is provided in GB 50010-2010 [53] and analyzed using SPSS software, as shown in equation (4). The test data and fitting results are shown in Figure 10.

$$f_{ts} = 0.07f_{cu}^{1.08}, \quad R^2 = 0.5682. \quad (4)$$

Figure 10 shows that the test data are consistent with the regression analysis data, indicating that the 28 days splitting tensile strength of RC subjected to early low-

Table 8: Compression regression model

T (°C)	Compression model	R^2
25	$f_{cu,28} = 36.74 + 1.13X_{BF} + 0.93X_{NS} - 0.18X_{BF}^2 - 0.19X_{NS}^2$	0.9684
0	$f_{cu,28} = 32.57 + 0.76X_{BF} + 1.87X_{NS} - 0.08X_{BF}^2 - 0.32X_{NS}^2$	0.9176
−10	$f_{cu,28} = 35.87 + 0.47X_{BF} + 1.67X_{NS} - 0.07X_{BF}^2 - 0.46X_{NS}^2$	0.9766
−20	$f_{cu,28} = 35.12 + 0.32X_{BF} + 2.27X_{NS} - 0.05X_{BF}^2 - 0.62X_{NS}^2$	0.8165

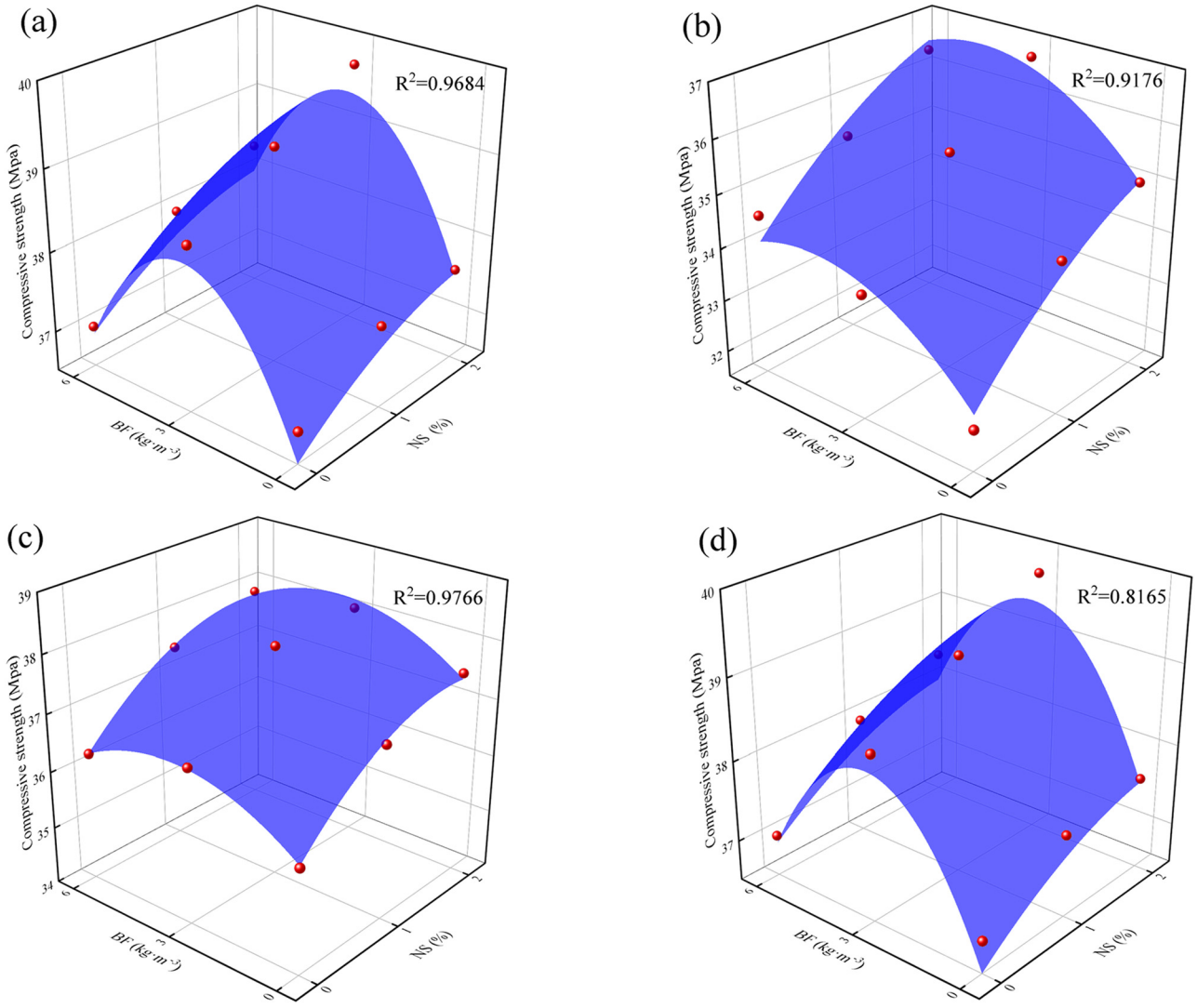

Figure 9: Data fitting of compressive strengths at different early temperatures: (a) 25°C, (b) 0°C, (c) −10°C, and (d) −20°C.

temperature environments can be predicted from the compressive strength using equation (4).

5 Microstructure

SEM helps in understanding the internal microscopic morphology of concrete and determining the crack extension. Figure 11 shows the SEM micrograph of RC under curing at 25°C. Under an electron microscope, the structure of the RC appears loose and obvious holes are observed. The three microcracks marked 1, 2, and 3 in the figure accelerate the damage development of the RC when it is damaged by force. The microcracks inside the RA and shrinkage cracks generated during the specimen casting and curing processes contribute to the low performance of the RC.

Combined with the results of the mechanical tests, four temperatures (−20, −10, 0, and 25°C) of B3N2 in the early stage were selected for SEM microanalysis, as shown in Figure 12. Figure 12a shows the RC micrographs of B3N2 in the early stage of 25°C maintenance. A comparison with Figure 11 indicates that BF and NS significantly improve the pores of RC. BF and free water in RC formed hydrogen bonds, and hydration products strengthened the connection between the fibers and substrate. The larger surface area and high reactivity of NS accelerated the hydration reaction. Numerous pores and microcracks existed inside the RC, and the NS suspension with the aggregate in the high-speed mixing was uniformly dispersed in the specimen as filler to fill the pores and cracks. Thus, the compactness of RC increased. Additionally, the volcanic ash effect, large specific surface area, and high reactivity of

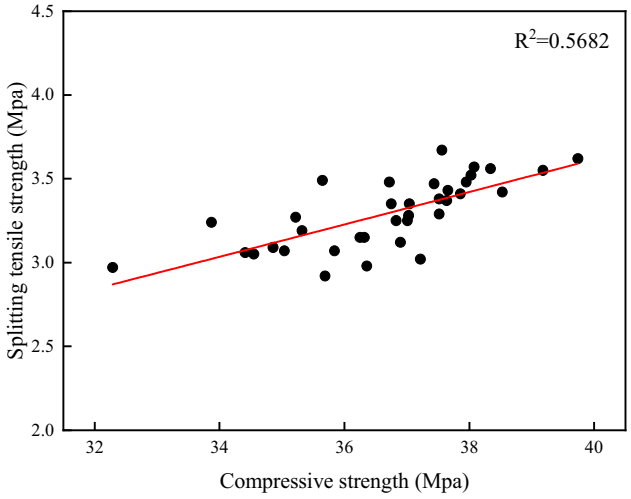

Figure 10: Relationship between the compression and splitting tensile strengths.

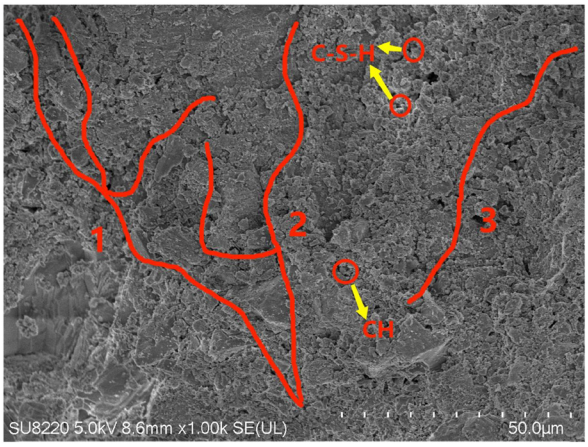

Figure 11: Image of RC under 25°C.

NS accelerated the hydration reaction of the cement and promoted the generation of hydration products C–S–H. This was dispersed as a matrix between the pores and cracks of RC and reduced its internal defects. Therefore, BF and NS reform the porosity of RC and improve its overall mechanical properties. A comparison between Figure 12a and b

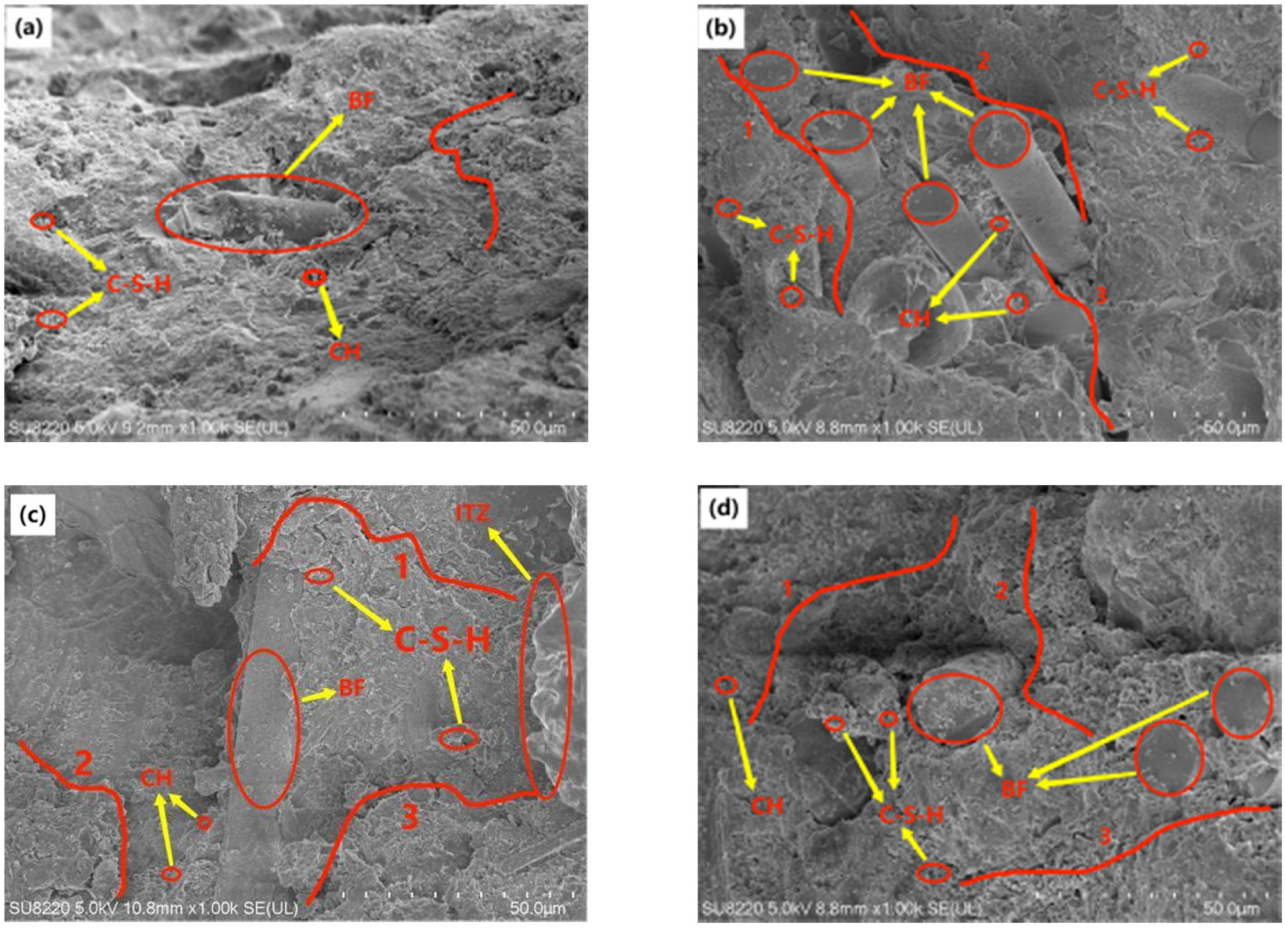

Figure 12: SEM images of B3N2 at various early temperatures: (a) 25°C, (b) 0°C, (c) −10°C, and (d) −20°C.

reveals that B3N2 causes serious damage in the 0°C low-temperature environment. Cracks appear in parts 1 and 2 in Figure 12b, and defects occur in the elliptical part. When subjected to external forces, the RC interior rapidly developed defects to the surface and eventually became damaged. Figure 12c shows the micrograph of B3N2 at −10°C, where three microcracks are labeled in the figure. The crack width is smaller than that at 0°C but larger than those at 25 and −10°C. The lowered temperature transformed water to ice in the B3N2. The expansion stress caused by freezing was not large, and the mortar and fibers of the bond between the fiber offset some of the stresses, while the NS filling of pore space and the hydration reactions promote the development of early strength, and prevented the development of the BF. The presence of NS mitigated the damage caused to RC by early low-temperatures. The presence of BF and NS alleviated the damage to the RC caused by low temperatures, and SEM results also verified the change in transformation in the macroscopic mechanical test. The micrograph of B3N2 at early −20°C (Figure 12d) shows that although BF is distributed in the RC, the cracks between the fibers and mortar are generated by the excessive freezing and expansion stress caused by the −20°C low-temperature environment. At −20°C, the water froze and could not participate in the hydration reaction, and the filling effect of NS was weakened by the expansion stress. Overall, the role of NS in RC in low-temperature environments was not obvious. When the temperature reached −20°C, frost expansion damage to early B3N2 occurred, and although some damage was repaired after transferring to the standard maintenance room, most of it was permanent. Therefore, the crack width of B3N2 at early −20°C shown in Figure 12d was higher than that caused by freezing and expansion in the early environment of −10°C, but lower than that caused by the environment of 0°C. Under external loading, the pores between the fibers served as the primary damage points and caused overall damage.

6 Conclusion

In this study, the changes in the mechanical properties and micromorphology of BF and NS modified RC in early low-temperature environments were investigated, and the main conclusions are as follows:

1) The RC was severely damaged, when subjected to external loading and an overall collapse was observed. BF and NS significantly improved the damage pattern of RC under compression, except for the shedding of the surface layer. The internal connection between the various parts did not suffer major damage, and the overall integrity improved.
2) Early low-temperature environments degraded the physical properties of RC. For example, 0°C had the greatest impact on the early physical properties; the mechanical properties first increased and then decreased with the temperature. The physical properties of RC at different early temperatures in descending order were: 25°C > −10°C > −20°C > 0°C.
3) BF effectively improved the physical properties of RC in the early low-temperature environment. The physical properties of RC first increased and then decreased with BF doping. When the BF doping was 3 kg m^{-3}, the compressive strength and splitting tensile strength of RC were the largest, and they reduced when the BF was 6 kg m^{-3}.
4) The doping of NS improved the performance of RC. The compressive strength and splitting tensile strength of RC increased with NS doping, and its compressive strength and splitting tensile strength at 2% NS doping improved by up to 10.4 and 19%, respectively, compared with those at 0% NS.
5) Owing to the good synergistic effects of BF and NS, the physical properties of RC were improved by compound doping of BF and NS. The compressive strength and splitting tensile strength increased to 18.1 and 22.3%, respectively, with the optimal dosages of 3 kg m^{-3} BF and 2% NS. This significantly reduced the internal defects of RC, strengthened the tight connection in the internal matrix of RC, and improved the overall density.
6) An expression for the 28 days compressive strength of RC was fitted using SPSS software.
7) BF and NS can reduce the number of pores in RC, and as the early ambient temperature decreased, the BF and mortar bond first decreased, then increased, and then decreased again. The 0°C low-temperature environment caused the largest damage cracks.

Funding information: This project was supported by the National Natural Science Foundation (51608179).

Author contributions: All authors have accepted the responsibility for the entire content of this manuscript and approved its submission.

Conflict of interest: The authors state no conflict of interest.

References

[1] Klepa RB, Medeiros MF, Franco MAC, Tamberg ET, Farias TMDB, Paschoalin Filho JA, et al. Reuse of construction waste to produce

thermoluminescent sensors for use in highway traffic control. J Clean Prod. 2019;209:250–8.
[2] Tang Y, Wang Y, Wu D, Chen M, Pang L, Sun J, et al. Exploring temperature-resilient recycled aggregate concrete with waste rubber: An experimental and multi-objective optimization analysis. Rev Adv Mater Sci. 2023;62(1):20230347.
[3] Xiao J, Shen J, Bai M, Gao Q, Wu Y. Reuse of construction spoil in China: Current status and future opportunities. J Clean Prod. 2021;290:125742.
[4] Esa MR, Halog A, Rigamonti L. Strategies for minimizing construction and demolition wastes in Malaysia. Resour Conserv Recycl. 2017;120:219–29.
[5] Zhao Y, Gao J, Chen F, Liu C, Chen X. Utilization of waste clay bricks as coarse and fine aggregates for the preparation of lightweight aggregate concrete. J Clean Prod. 2018;201:706–15.
[6] Behera M, Bhattacharyya SK, Minocha AK, Deoliya R, Maiti S. Recycled aggregate from C&D waste & its use in concrete a breakthrough towards sustainability in construction sector: A review. Constr Build Mater. 2014;68:501–16.
[7] Lee H, Choi MK, Kim B. Structural and functional properties of fiber reinforced concrete composites for construction applications. J Ind Eng Chem. 2023;125:38–49.
[8] Algin Z, Ozen M. The properties of chopped basalt fibre reinforced self-compacting concrete. Constr Build Mater. 2018;186:678–85.
[9] Li Z, Shen A, Zeng G, Chen Z, Guo Y. Research progress on properties of basalt fiber-reinforced cement concrete. Mater Today Commun. 2022;33:104824.
[10] Yuan J, Shen D, Xu Z, Li M, Wen C, Zong D. Effect of bond length on bond behavior between basalt fiber-reinforced polymer sheet and concrete. Constr Build Mater. 2023;392:131586.
[11] Zheng Y, Zhuo J, Zhang Y, Zhang P. Mechanical properties and microstructure of nano-SiO_2 and basalt-fiber reinforced recycled aggregate concrete. Nanotechnol Rev. 2022;11(1):2169–89.
[12] Fang S, Hong H, Zhang P. Mechanical property tests and strength formulas of basalt fiber reinforced recycled aggregate concrete. Materials (Basel). 2018;11(10):1851.
[13] Yang Y, Fang S, Feng W, Wan S, Li L, Tang Y. Flexural and compressive performance of BFRP-reinforced geopolymer sea-sand concrete beams and columns: Experimental and analytical investigation. Compos Struct. 2023;318:117089.
[14] Zheng Y, Zhuo J, Zhang P, Ma M. Mechanical properties and mesomicroscopic mechanism of basalt fiber-reinforced recycled aggregate concrete. J Clean Prod. 2022;370:133555.
[15] Chen Z, Yu J, Nong Y, Yang Y, Zhang H, Tang Y. Beyond time: Enhancing corrosion resistance of geopolymer concrete and BFRP bars in seawater. Compos Struct. 2023;322:117439.
[16] Zhang C, Wang Y, Zhang X, Ding Y, Xu P. Mechanical properties and microstructure of basalt fiber-reinforced recycled concrete. J Clean Prod. 2021;278:123252.
[17] Wang Y, Cheng J, Wang J. Flexural performance of recycled concrete beam reinforced with modified basalt fiber and nano-silica. Case Stud Constr Mater. 2023;18:e02022.
[18] Borja W, Adarmouch M, El Hafiane Y, Daafi Y, Tamraoui Y, Alami J. Synthesis of nano-silica as a promising route of recycling phosphate waste rocks and its incorporation in mortars. Sustain Mater Technol. 2023;37:e00684.
[19] Li S, Hu M, Chen X, Sui S, Jin L, Geng Y, et al. The performance and functionalization of modified cementitious materials via nano titanium-dioxide: A review. Case Stud Constr Mater. 2023;19:e02414.
[20] Ali L, Ouni MHE, Raza A, Janjua S, Ahmad Z, Ali B, et al. Experimental investigation on the mechanical and fracture evaluation of carbon Fiber-reinforced cementitious composites with nano-calcium carbonate. Constr Build Mater. 2021;308:125095.
[21] Xavier CSB, Rahim A. Nano aluminium oxide geopolymer concrete: An experimental study. Mater Today: Proc. 2022;56:1643–7.
[22] Yan Y, Xing Z, Chen X, Xie Z, Zhang J, Chen Y. Axial compression performance of CFST columns reinforced by ultra-high-performance nano-concrete under long-term loading. Nanotechnol Rev. 2023;12(1):20220537.
[23] Mukharjee BB, Barai SV. Influence of incorporation of nano-silica and recycled aggregates on compressive strength and microstructure of concrete. Constr Build Mater. 2014;71:570–8.
[24] Said AM, Zeidan MS, Bassuoni MT, Tian Y. Properties of concrete incorporating nano-silica. Constr Build Mater. 2012;36:838–44.
[25] Nazari A, Riahi S. The role of SiO_2 nanoparticles and ground granulated blast furnace slag admixtures on physical, thermal and mechanical properties of self compacting concrete. Mater Sci Eng A. 2011;528(4–5):2149–57.
[26] Zhang Y, Zhu X. Effect of nano-silica on the mechanical performance and microstructure of silicon-aluminum based internal cured concrete. J Build Eng. 2023;65:105735.
[27] Rezaei F, Memarzadeh A, Davoodi M, Dashab M, Nematzadeh M. Mechanical features and durability of concrete incorporating recycled coarse aggregate and nano-silica: Experimental study, prediction, and optimization. J Build Eng. 2023;73:106715.
[28] Xu Z, Bai Z, Wu J, Long H, Deng H, Chen Z, et al. Microstructural characteristics and nano-modification of the interfacial transition zone in concrete: A review. Nanotechnol Rev. 2022;11(1):2078–100.
[29] Vijayan DS, Devarajan P, Sivasuriyan A. A review on eminent application and performance of nano based silica and silica fume in the cement concrete. Sustain Energy Technol Assess. 2023;56:103105.
[30] Wang Y, Hughes P, Niu H, Fan Y. A new method to improve the properties of recycled aggregate concrete: Composite addition of basalt fiber and nano-silica. J Clean Prod. 2019;236:117602.
[31] Yi S, Pae S, Kim J. Minimum curing time prediction of early-age concrete to prevent frost damage. Constr Build Mater. 2011;25(3):1439–49.
[32] Xia W, Cui S, Zhu L, Li W, Woody Ju J, Wang X. Effects of nano-silica modification on early age hydration process in winter construction of tunnel engineering. Constr Build Mater. 2023;408:133804.
[33] Zhang G, Yu H, Li H, Yang Y. Experimental study of deformation of early age concrete suffering from frost damage. Constr Build Mater. 2019;215:410–21.
[34] Dong S, Feng D, Jiang S, Zhu W. Effect of freezing temperature on the microstructure of negative temperature concrete. Adv Mat Res. 2013;663:343–8.
[35] Dai J, Wang Q, Zhang B. Frost resistance and life prediction of equal strength concrete under negative temperature curing. Constr Build Mater. 2023;396:132278.
[36] Mohan MK, Rahul AV, Van Stappen JF, Cnudde V, De Schutter G, Van Tittelboom K. Assessment of pore structure characteristics and tortuosity of 3D printed concrete using mercury intrusion porosimetry and X-ray tomography. Cem Concr Compos. 2023;140:105104.
[37] Wang Y, Yang S, Luo Q, Li Q, Sun G. Experimental characterization of impact damage in foam-core sandwich structures using acoustic emission, optical scanning and X-ray computed tomography techniques. Compos Part B: Eng. 2023;265:110919.

[38] Li G, Chen X, Zhang Y, Zhuang Z, Lv Y. Studies of nano-SiO_2 and subsequent water curing on enhancing the frost resistance of autoclaved PHC pipe pile concrete. J Build Eng. 2023;69:106209.
[39] Chen C, Lu C, Lu C, Wei S, Guo Z, Zhou Q, et al. Synergetic effect of fly ash and ground-granulated blast slag on improving the chloride permeability and freeze–thaw resistance of recycled aggregate concrete. Constr Build Mater. 2023;365:130015.
[40] Cai Y, Zhang Y, Liu Y, Li J. Predictive method for the macroscopic mechanical properties of concrete at ultra-low temperatures. Constr Build Mater. 2022;357:129276.
[41] Wang D, Lu C, Zhu Z, Zhang Z, Liu S, Ji Y, et al. Mechanical performance of recycled aggregate concrete in green civil engineering: Review. Case Stud Constr Mater. 2023;19:2384.
[42] Ji T. Preliminary study on the water permeability and microstructure of concrete incorporating nano-SiO_2. Cem Concr Res. 2005;35(10):1943–7.
[43] Standardization administration of China, Standard for test methods of physical and mechanical properties of concrete, GB/T 50081-2019. Beijing: China Construction Industry Press; 2019.
[44] Shatarat N, Katkhuda H, Ayyoub M, Al-Hunaiti Y, Abdel Jaber MS. Improving bond strength of recycled coarse aggregate concrete using chopped basalt fibers. Case Stud Constr Mater. 2022;17:1449.
[45] Nigam M, Verma M. Effect of nano-silica on the fresh and mechanical properties of conventional concrete. Forces Mech. 2023;10:100165.
[46] Adessina A, Fraj AB, Barthélémy J. Improvement of the compressive strength of recycled aggregate concretes and relative effects on durability properties. Constr Build Mater. 2023;384:131447.
[47] Dilbas H, Çakır Ö. Influence of basalt fiber on physical and mechanical properties of treated recycled aggregate concrete. Constr Build Mater. 2020;254:119216.
[48] Roy C, Mohanty T, Kumar Bera D. Effectiveness of nano silica on properties of self-compacting concrete. Mater Today: Proc. 2023;7:273.
[49] Harish BA, Hanumesh BM, Venkata Ramana N, Gnaneswar K. Assessment of mechanical properties of recycled coarse aggregate concrete incorporating basalt and polypropylene fiber. Mater Today: Proc. 2023;6:196.
[50] Zhang H, Ji S, Wang L, Jin C, Liu X, Li X. Study on dynamic splitting tensile damage characteristics of basalt fiber reinforced concrete based on AE and DSCM. J Build Eng. 2022;57:104905.
[51] Zhu L, Wen T, Tian L. Size effects in compressive and splitting tensile strengths of polypropylene fiber recycled aggregate concrete. Constr Build Mater. 2022;341:127878.
[52] Khodair Y, Bommareddy B. Self-consolidating concrete using recycled concrete aggregate and high volume of fly ash, and slag. Constr Build Mater. 2017;153:307–16.
[53] Ministry of Housing and Urban-Rural Development of the People's Republic of China. Design code for concrete structures: GB 50010-2010. Beijing: China Building Industry Press; 2010.